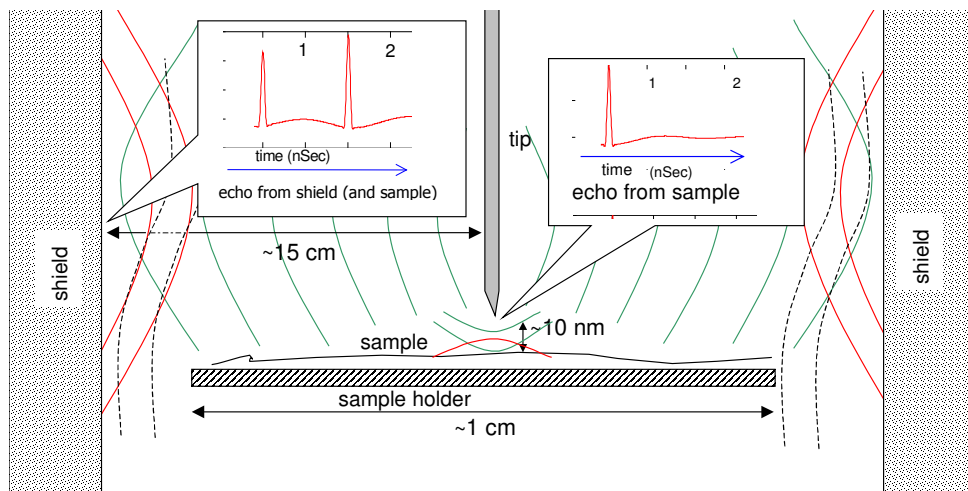


## Materials and Methods



**Fig. S1:** Some typical distances/sizes of the microscope (not to scale; dimensions are only meant as orders of magnitude) and illustration of the basic principle: the tip irradiates by its whole body (green: incident waves; red: reflected waves). After Fourier anti-transform of the measured reflection coefficient, one obtains the response of the system to a synthetic time pulse, namely a set of echoes. Echoes originating from the microscope body (here only the main echo due to the metal shield is shown) are distinguished from the echoes originating by the sample.

### Instrumental Setup

We have modified two commercial instruments: a Scanning Tunneling Microscope (STM), an NT-MDT P-47 Solver, and a Vector Network Analyzer Agilent E8361A (VNA), used to perform ultra-broad band measurements of the microwave signal with high dynamic (bandwidth 70GHz, dynamical range 120dB). Figure 1 in the letter shows how they are connected and a detail of how we have realized the microwave/STM head (also in video EPAPS No. 1).

An home-made program synchronizes the STM and the acquisition from the VNA. Basically, the sample is horizontally displaced by a piezo membrane (xy), and the reflection coefficient is read through an Ethernet connection. The VNA performs a frequency sweep over a sub-band of the 0-70 GHz capability. The STM controller keeps the sample/probe distance by changing the z-position of the piezo-membrane, and ensuring a predefined tunnel current. By reading the z-position, a simultaneous STM topographical map is obtained. In order to perform also a simultaneous "Local Barrier-Height" spectroscopy, namely an image  $dI/dz$  (derivative of the tunnel current with respect to changes in height), an additional lock-in is used: a low-frequency oscillating signal (7-8 kHz: the period much smaller than the time constant of the feedback loop in the STM) is applied to the piezoelectric membrane and the amplitude of the oscillation in the tunneling current is detected by the lock-in chain, providing an image proportional to  $dI/dz$ .

At the end of the scan, we have an STM topographic image, a local barrier-height spectroscopic image and several microwave images (usually more than 500) at different frequencies.

The same software performs calibration and time-domain transform(see next sections).

Note that, unlike the systems presented in the literature, no resonator has been inserted in the microwave head.

### Preparation of C2C12 samples

C2C12 cells (American Type Culture Collection, ATCC, Rockville, MD; CRL 1772) were cultured as exponentially growing myoblasts in growth medium (GM, Pietrangelo et al (1)). Cells were seeded on HOPG substrates in Petri dishes at a density of 1500–2000 cells cm<sup>-2</sup> and after two days in GM, differentiation was induced shifting GM with differentiation medium (DM) containing DMEM with 2% horse serum (Euroclone), L-glutamine and antibiotics. After 5-6 days of differentiation the cells become multinucleated syncytia named myotubes. Part of myotubes were directly rinsed and analysed (fig. S6), other myotubes were fixed for 10 min by slowly adding 3.7% paraformaldehyde (Sigma-Aldrich), then rinsed and analyzed (figs. 5 and S6).

### Calibration and Quantitative measurements

While not always necessary for the purpose of imaging (data presented for biological experiments in the paper are raw), frequency domain data can be first calibrated. Microwave calibration is performed off-line (post-processing) in our software, in order to reduce the acquisition time, by exploiting three arbitrary known loads, and by recovering the two-port error matrix, that is an admittance  $Y_e$ -matrix given by:

$$y_{e11} = \frac{N_{11}}{\Delta} \quad y_{e12} = \frac{N_{12}}{\Delta} = y_{e21} \quad y_{e22} = \frac{N_{22}}{\Delta} \quad \text{with}$$

$$N_{11} = [(y_{L2} - y_{L3})y_{i3} + (y_{L1} - y_{L2})y_{i1}]y_{i2} + (y_{L3} - y_{L1})y_{i1}y_{i3}$$

$$N_{22} = (y_{L1} - y_{L2})y_{L3}y_{i3} + (y_{L3} - y_{L1})y_{L2}y_{i2} + (y_{L2} - y_{L3})y_{L1}y_{i1}$$

$$N_{12} = \pm \sqrt{(y_{L1} - y_{L3})(y_{i2} - y_{i1})(y_{L3}y_{L1} - y_{L1}y_{L2} + y_{L2}^2 - y_{L3}y_{L2})(y_{i1}y_{i2} - y_{i2}y_{i3} + y_{i3}^2 - y_{i1}y_{i3})}$$

$$\Delta = y_{i1}(y_{L3} - y_{L2}) + y_{i2}(y_{L1} - y_{L3}) + y_{i3}(y_{L2} - y_{L1})$$

In the above  $y_{Li}$  are the known admittance loads (standards), and  $y_i$  are the correspondent raw data measured by the VNA. Note that there is a sign indetermination in  $y_{e12}$ , but this does not affect the calibration as in the input admittance  $y_{e12}$  appears squared.

The effect of  $Y_e$  is removed by creating a new  $Y_c$ , with elements

$$y_{c1,1} = -y_{e2,2}, y_{c1,2} = -y_{e2,1}, y_{c2,1} = -y_{e1,2}, y_{c2,2} = -y_{e1,1},$$

and by connecting the resulting  $Y_c$  to the measured bipole.

The selection of the known loads defines the reference plane where the quantitative measurement is performed: calibrating at the head of the microwave scanner is just a standard calibration process performed by the commercial VNA calibration kit.

However if we are interested into a frequency domain quantitative measurement, we do need to shift the reference plane at the end of the tunnel tip. This can be done only by known loads to be presented to such a tip, with all the issues discussed in the manuscript.

A possibility, that we will discuss in detail in a dedicated paper, is to use part of the tip itself as known load: the end of the tip can be approximated by a sphere having a curvature radius estimated by a SEM imaging of the tip. Hence our known loads can be

$$y_i^{(L)} = j\omega C_i = j\omega 4\pi\epsilon \sqrt{(d_i + a)^2 - a^2} \cdot$$

$$\sum_{n=0}^{\infty} \left\{ \coth \left[ \left( n + \frac{1}{2} \right) \operatorname{acosh} \left( \frac{d_i + a}{a} \right) \right] - 1 \right\}$$

where  $i$  is the index of the load and ranges from 1 to 3,  $d_i$  are the sphere/ground distances and  $a$  the estimated curvature radius.

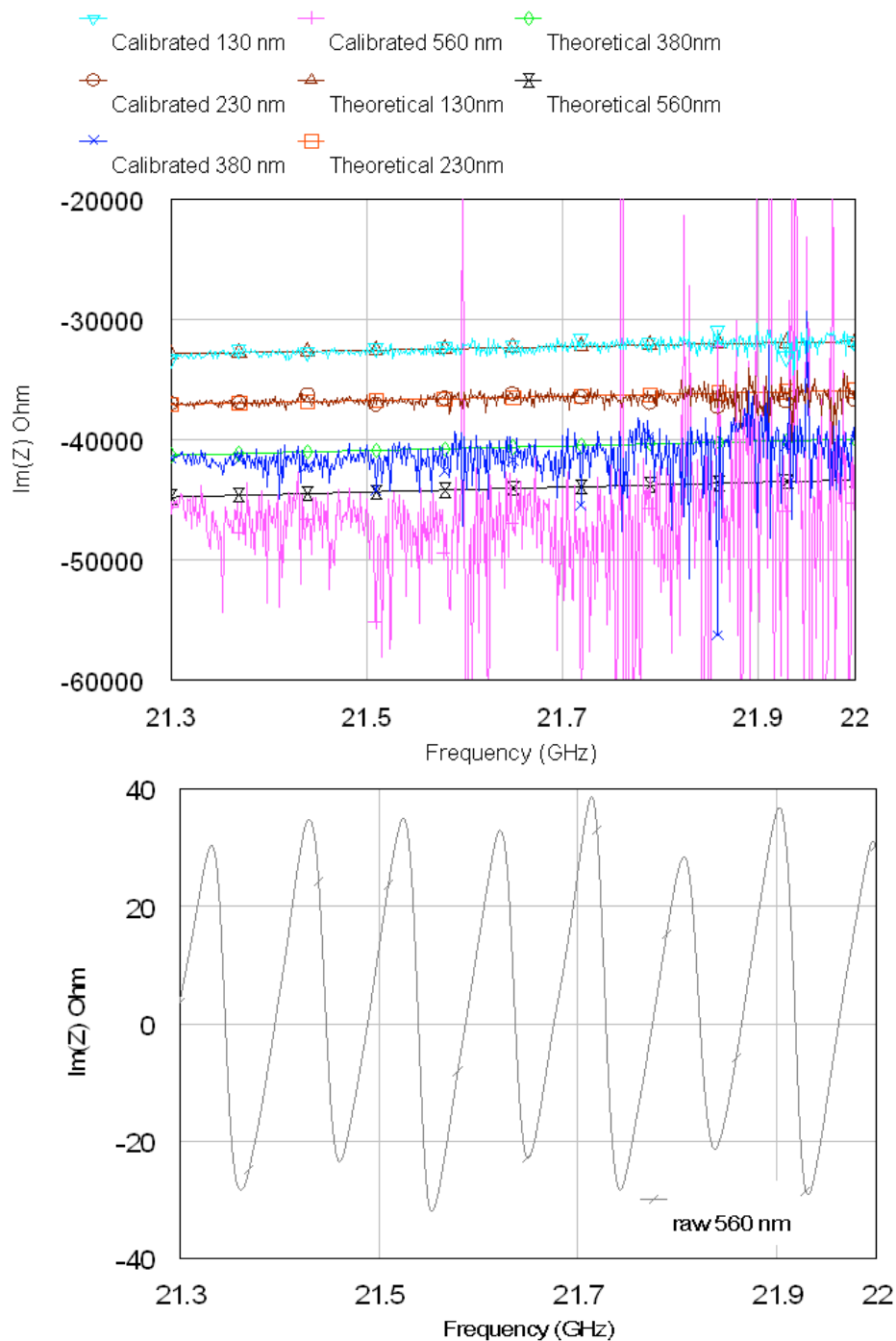


**Fig. S2:** (up) Comparison between measured impedance after calibration over an HOPG sample, and predicted impedance after the spherical capacitance model, at different quotes. Match is almost excellent below 21.5 GHz. (down) Measured impedance before calibration: all quotes are visually coincident; hence only one quote is reported

By performing measurements at three known distances from the sample we have the three known loads. From a practical point of view, if a sample is deposited on a conducting substrate (e.g. HOPG, conducting glass etc), part of the substrate is kept clean for the purpose of calibration. Note that, while

in many papers this capacitive model of the tip has been used in quantitative microwave measurements, to the best of our knowledge it has never been adopted in a systematic calibration process as the one described here. In fact, a spherical capacitance model was usually used only to estimate the change in the permittivity  $\epsilon$  (see e.g. the review by Gao et al. [1]). In our case, such capacitances are calibration loads allowing the quantitative measurement of the admittance seen at tip end.

The main non trivial issue is to have a reliable measurement of the *absolute* tip-to-sample distance. The relative distance is usually well known in an STM system, and can be changed reliably by a lock-in device (in our case included in the NT-MDT microscope). The zero distance, namely the one corresponding to the "contact" condition of tip-to-sample, is detected by plotting I-V characteristics and searching for the transition from tunnel (exponential) to Ohm (linear) regime, reading the quote from the lock-in device (or the piezo membrane displacement). Of course, the detection of the "zero" is the latest measurement in the post-process, as it likely damages the tip.

Most remarkably, such an approach also provides analytically known loads to be used in a test about the quality of the calibration process: we can perform measurements at different quotes and compare the measured admittances with the ones predicted by the capacitance model. A marked departure from the expected value is a symptom of a frequency range where parasitic mechanisms are dominating (the interaction between tip and sample is mediated by parasitic paths, as discussed in the paper). The sphere-to-ground model is known to be excellent within several hundreds of nanometers of tip-to-sample distance [2]. In the figure S2 we can see a comparison between the measured (calibrated) impedance and the impedance predicted considering the spherical capacitance (curvature radius around 1  $\mu\text{m}$ ) at the measured tip-to-sample distance.

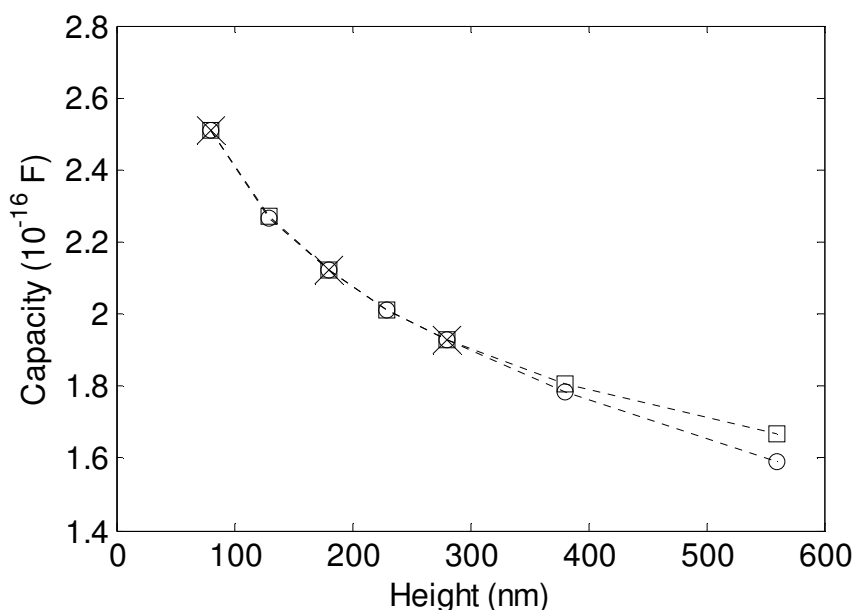


**Fig. S3:** Comparison between the tip-sample capacitances calculated by a quasi static model (squares), i.e. a metallic sphere placed at different heights above a perfect conducting plane, and the capacitances calculated by our calibration procedure (circles).

In the calibration curve a spherical-tip approximation is still applied, but only to three of the seven selected heights: the capacitances corresponding to these calibration points, marked with 1, 3 and 5 (indicated by Xs), are then coincident with those of the other curve. The capacitances at heights 2, 4, 6 and 7 are extrapolated by the described calibration procedure and show good agreement with the spherical model. The above results suggest that the proposed procedure works well if combined with a spherical geometry for the tip, at least for small displacements from the calibration heights

This is plotted over a small transition frequency range, where image quality starts to deteriorate (around 21.5 GHz); note that between 21.9 GHz and 22 GHz the SMM was almost blind indicating either that undesired paths are dominating or that the system sensitivity drops down for a large reflection of the wave before the tip-sample interface.

In our experience an agreement between theoretical and measured data in the order of 1-3% spans usually several GHz. A direct comparison between the theoretical capacitance and the one obtained by fitting the imaginary part of the admittance is reported in figure S3.

### Time domain

In order to obtain time-domain data, the frequency domain responses are linearly combined according to

$$s(t) = \sum_{f_i} \text{Re}(K(f_i)S(f_i)e^{j2\pi f_i t})$$

where  $f_i$  are the available frequencies,  $S(f)$  is the reflection coefficient recorded in frequency domain and  $K(f)$  is a weighting function. In our work we used for  $K(f)$  the Kaiser-Beta windowing function. Whenever  $f_i$  are equally spaced frequencies spanning from 0 to maximum frequency  $f_{max}$ , the above becomes a standard finite Fourier transform providing the response to a synthesized impulse having approximate width  $1/(f_{max})$  (the Kaiser-Beta usually broadens the pulse).

Table I

Symbol	Value	Unit
Cc	55.8	fF
Coax	Inner conductor 600	μm
	Outer conductor 2.62	mm
	Er 2.12	
TL1	Length 13.6	mm
	Length 104	Deg
	@ 10	GHz
TL2	Zo 792	Ohm
	Length 3.38	Deg
	@ 30	GHz
TL3	Zo 27540	Ohm
	Length 8.575	Deg
	@ 30	GHz
TL4	Zo 22940	Ohm
	Length 3.83	Deg
	@ 50	GHz
TL5	Zo 19940	Ohm
	Length 4.19	Deg
	@ 60	GHz
TL6	Zo 22940	Ohm
	Length 347.5	Deg
	@ 70	GHz
R1	Zo 22640	Ohm
	657	Ohm
R2	20.5	Ohm
R3	51.3	Ohm
R4	46.2	Ohm
R5	42.2	Ohm
R6	1000	Ohm
C1	8.8	fF
C2	13.9	fF
C3	11.4	fF
C4	12.4	fF
C5	18.1	fF

C6	18.3	fF
Csample	0.7	fF
RTunnel	75	KOhm

---

### *Additional data*

STM provides a topographic image where large corrugations could hide small details; in order to make visible such details, as stated in the text, STM images were processed by a standard "fit line procedure"; nonetheless smaller details may still be barely visible.

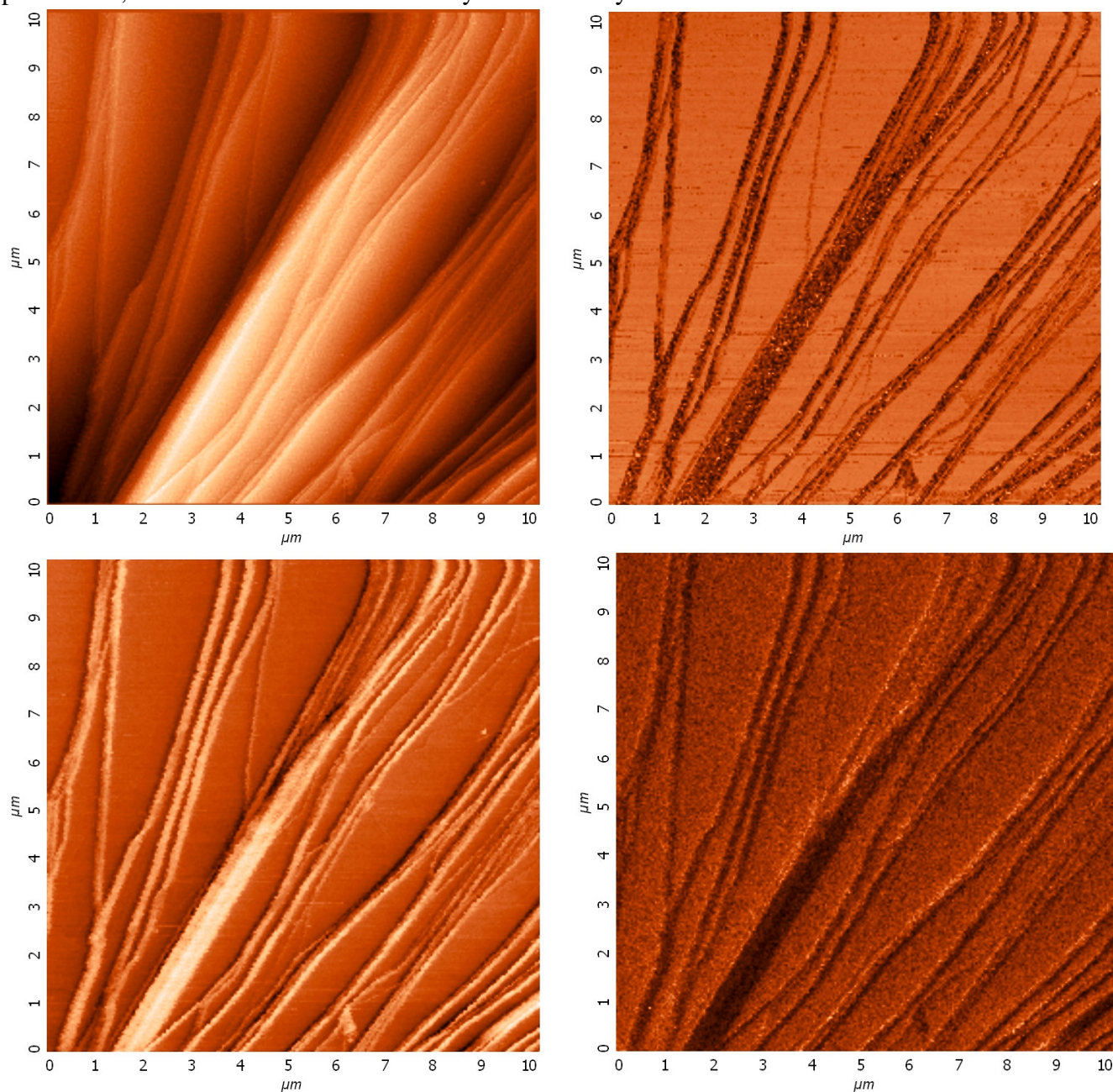


**Fig. S4:** *Up left: STM topographical image of an HOPG sample; Up right:  $dI/dz$  spectroscopic image; Bottom left: time domain microwave image at 10.4nS; Bottom right: frequency domain image at 21.456 GHz (magnitude); such a frequency was one among a group of frequencies ( in the considered small range 21.3-22 GHz, 512 points) featuring images with acceptable quality*

In order to overcome this limit, the images in figure S4 show the STM topographical plot (corrected), a spectroscopic  $dI/dz$  image, a time-domain ( $t=10.4\text{ns}$ ; uncalibrated data) microwave image and a frequency domain ( $f=21.3\text{GHz}$ ) microwave image of the same HOPG sample. Images were obtained simultaneously, during the same raster scan. The time-domain image was obtained by processing a quite narrow frequency band (21.3-22 GHz), nonetheless the quality obtained is remarkable when compared with the unprocessed frequency-domain image: this can be understood considering the time behavior of a few sinusoids interfering (see figure S5).

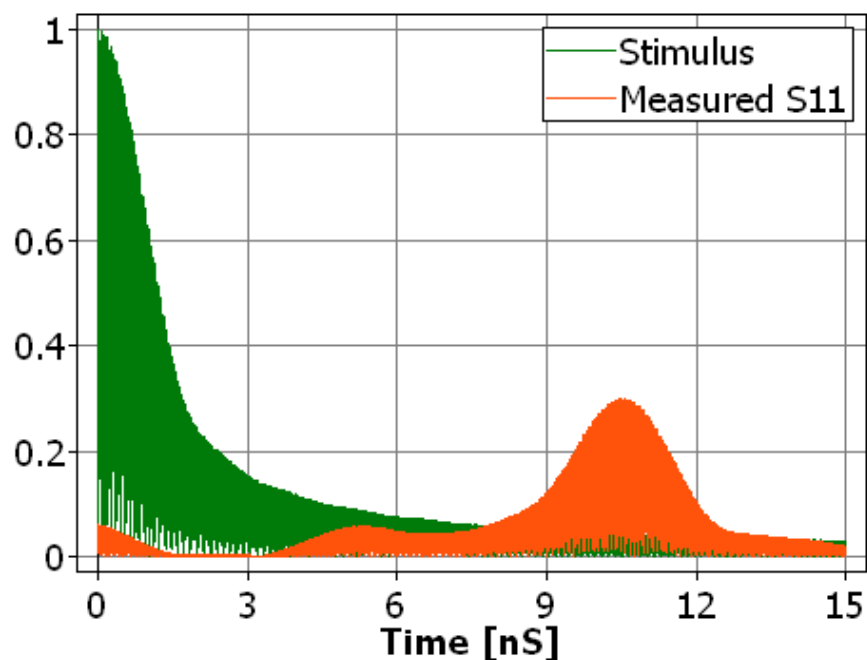


**Fig. S5:** Time-domain pulse and measured response corresponding to 512 equispaced frequency points in the range 21.3- 22GHz.

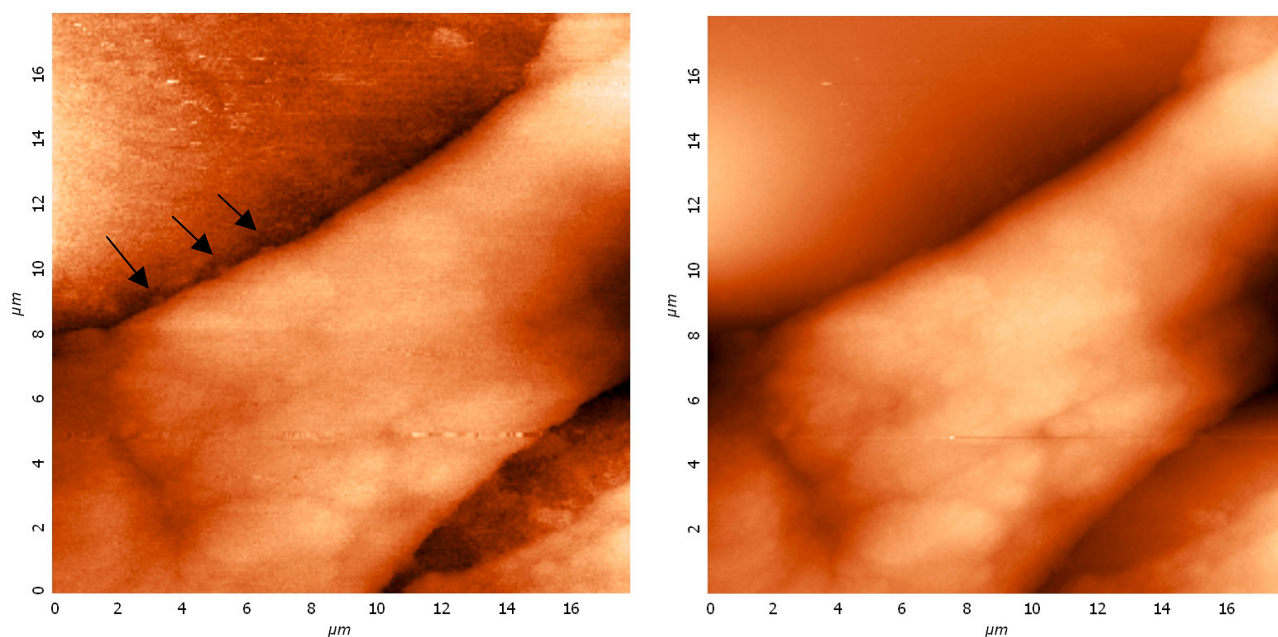


**Fig. S6:** Zoom of myotubes fixed with paraformaldehyde on HOPG substrate. Left: time-domain microwave image; right: STM. Arrows indicate details in the microwave image partially hidden in the STM one.

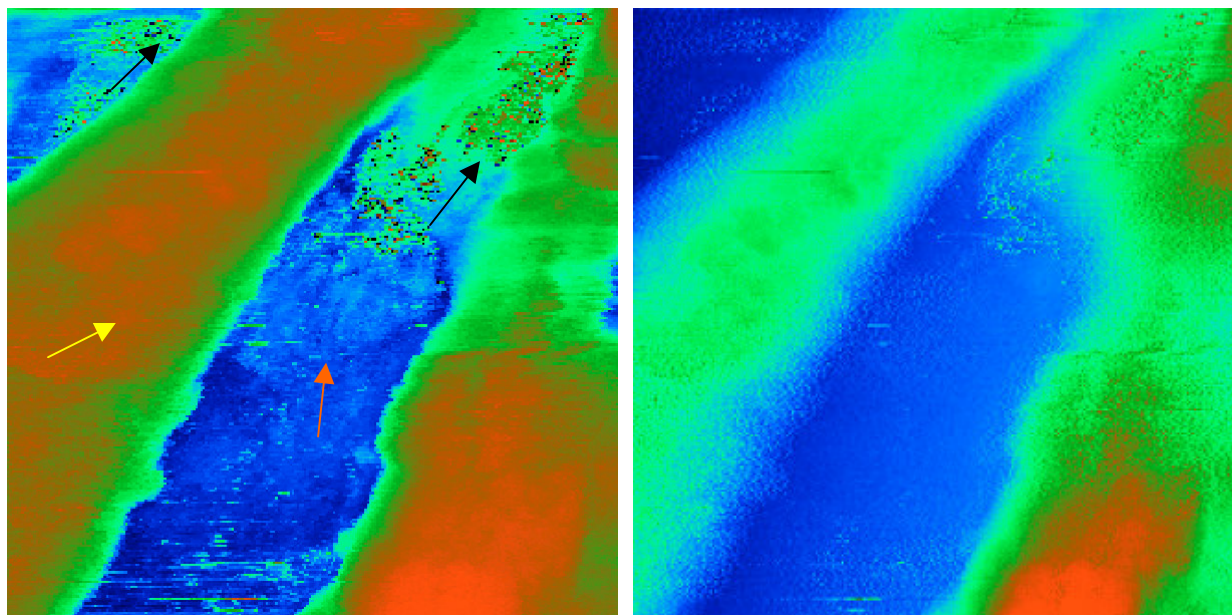


**Fig. S7:** Comparison for living myotubes. Left: time-domain microwave image; right STM image. Black arrows: saline crystals. Orange arrow: extracellular fluids. Yellow arrow: nuclei.

The last two figures are further examples of measurements over cells, both fixed and living. Figure S6 in particular is a zoom of a region of the fixed cells shown in the letter.

In fig. S7, featuring living cells, the tunneling image appears quite noisy, mostly owing to issues of the feedback of our specific STM instrument, unable to work properly with very low currents near the limit of our STM head; moreover the microwave cable adds some mechanical vibration; nonetheless the time-domain microwave scan shows interesting features. The latter in fact also identifies some of the fluids surrounding the cell (cells are dying as no longer in their physiological buffer), while there are saline crystals inducing high reflectivity contrasts. Likely also nuclei of cells (yellow arrow) are visible.

#### Materials and Methods: References

1. C. Gao et al.: "Quantitative scanning evanescent microwave microscopy and its applications in characterization of functional materials libraries", *Meas. Sci. Technol.* **16**248–260, (2005).
2. S. Kurokawa and A. Sakai, "Tip-Sample Capacitance in STM", *Sci. Rep. RITU* **A44-2**, 173-179 (1997)
3. T. Pietrangelo et. al , Extracellular guanosine-5'-triphosphate modulates myogenesis via intermediate Ca<sup>2+</sup>-activated K<sup>+</sup> currents in C2C12 mouse cells. *J Physiol* **572.3**, 721-733 (2006).